Title

Amino-terminal domain stability mediates apolipoprotein E aggregation into neurotoxic fibrils

Journal

Journal of Molecular Biology, 361(5)

ISSN

0022-2836

Authors

Hatters, Danny M
Zhong, Ning
Rutenber, Earl
et al.

Publication Date

2006-09-01

Peer reviewed

Amino-terminal Domain Stability Mediates Apolipoprotein E Aggregation Into Neurotoxic Fibrils

Danny M. Hatters, Ning Zhong, Earl Rutenber and Karl H. Weisgraber*

Gladstone Institute of Neurological Disease, 1650 Owens St., San Francisco, California 94158 USA and University of California, San Francisco, California 94143, USA

Running title: Isoform-specific rates of apoE aggregation

*Corresponding author

E-mail address of the corresponding author: kweisgraber@gladstone.ucsf.edu

SUMMARY

The three isoforms of apolipoprotein (apo) E are strongly associated with different risks for Alzheimer's disease: apoE4 > apoE3 > apoE2. Here, we show at physiological salt concentrations and pH that native tetramers of apoE form soluble aggregates *in vitro* that bind the amyloid dyes thioflavin T and Congo Red. However, unlike classic amyloid fibrils, the aggregates adopt an irregular protofilament-like morphology and are mostly α-helical. The aggregates formed at substantially different rates (apoE4 > apoE3 > apoE2) and were significantly more toxic to cultured neuronal cells than the tetramer. Since the three isoforms have large differences in conformational stability that can influence aggregation and amyloid pathways, we tested the effects of mutations that increased or decreased stability. Decreasing the conformational stability of the amino-terminal domain of apoE increased aggregation rates and *vice versa.* Our findings provide a new perspective for an isoform-specific pathogenic role for apoE aggregation in which differences in the conformational stability of the amino-terminal domain mediate neurodegeneration.

Keywords: Alzheimer's disease;Amyloid;Apolipoproteins;Protein misfolding, Aggregate toxicity.

Abbreviations used: AB, 100 mM NH_4HCO_3, pH 7.8; apo, apolipoprotein; AD, Alzheimer's disease; APP, amyloid precursor protein; CD, circular dichroism; CSF, cerebrospinal fluid; GFAP, glial fibrillary acidic protein; MTT, 3-(4,5-dimethylthiazol-2-yl)-2,5-diphenyltetrazolium bromide; PBS, 135 mM NaCl, 2.7 mM KCl, 4.3 mM Na_2HPO_4, 1.4 mM KH_2PO_4, pH 7.4; TBS, 10 mM Tris, 150 mM NaCl, 0.25 mM EDTA, 0.05% NaN_3, pH 7.4; vHW, van Holde-Weischet.

INTRODUCTION

Aplipoprotein E genotype is a major genetic determinant for the risk of developing Alzheimer's disease (AD). Of the three common allelic isoforms, apoE4 confers greater risk and apoE2 less risk than apoE3 [1]. The isoforms (299 amino acids) differ in sequence at only amino acids 112 and 158: apoE3 has cysteine and arginine, respectively while apoE2 has cysteines at both positions and apoE4 arginines [2].

How these sequence differences influence AD is not well understood. Several different, and possibly distinct mechanisms have been proposed including the formation of neurotoxic proteolytic fragments of apoE, the binding of apoE to Aβ and mediation of fibrillization and plaque formation, the binding and disruption of membranes by apoE, apoE-mediated lipid transport, and apoE-mediated neuronal sensitivity to injury and recovery [3-11].

One striking feature of apoE is the direct association with amyloid deposition and plaque load in AD. In postmortem AD brain sections, apoE4 is associated with greater Aβ deposition, amyloid dye reactivity, and density of neuritic plaques than apoE3 [12]. Transgenic mouse models of AD also show that apoE is central to influencing Aβ amyloid plaque pathology and deposition [6, 11]. Older transgenic mice expressing the V717F mutant of amyloid precursor protein (APP) develop significantly greater quantities of thioflavin-S-reactive neuritic plaques in the hippocampus when also expressing human apoE in astrocytes under the glial fibrillary acidic protein (GFAP) promoter [6]. ApoE4 also produces a more severe phenotype than apoE3, and the lack of apoE results in more diffuse deposits that do not react with thioflavin S [6]. Thus, apoE may be necessary for the formation of Aβ aggregates with a fibrillar amyloid structure characteristic of AD pathology.

Could apoE itself form amyloid-like aggregates in physiological buffers? ApoE and its fragments are components of amyloid-rich fractions of brain tissue, and an apoE fragment consisting of amino acids 216–299 forms fibrillar structures *in vitro* [13, 14]. ApoE is also associated with almost all types of systemic and peripheral amyloidoses that are caused by unrelated proteins [15-19]. In addition, other apolipoproteins or structurally similar proteins, including apoA-I, apoA-II, apoC-II, serum amyloid A, and α-synuclein, are associated with amyloidoses or form fibrils *in vitro*, suggesting that the common structural properties of apolipoproteins result in a general propensity for misfolding and self-association [20].

RESULTS

We found that refolding apoE by dialysis or gel filtration chromatography from chaotropes results in a variable mixture of higher and lower mass apoE. Previous studies have shown an equilibrium of different species of apoE, consisting predominately of tetramers and octamers, with minor amounts of dimer, monomer, and larger oligomers/aggregates [21-23]. To

avoid the confounding effects of pre-existing aggregates and misfolded protein, we removed the higher mass material by gel filtration chromatography and retained the predominant lower mass peak.

To investigate the homogeneity of the lower mass apoE4 we performed sedimentation velocity analysis and used two approaches to analyse the data (Figure 1a). First, we used the van Holde-Weischet (vHW) method that provides a diagnostic tool for sedimentation behaviour based on a model-free assessment of the range of sedimentation coefficients [24]. vHW analysis revealed a narrow range of sedimentation coefficients of 4–6 S, centred at about 5 S, which is consistent with near-homogeneity (Figure 1b). This suggests the presence of either tetramer or octomer (or both), since both species are likely to have a sedimentation coefficient in the range of 4–7 S [23]. Second, we used *c*(*s*) analysis, which provides a more quantitative assessment of the species present and models the sedimentation boundaries directly to a continuous distribution of solutions to the Lamm equation [25]. This analysis gave a sharp single peak of sedimentation coefficients centred at 5.2 S (Figure 1a and 1b). While *c*(*s*) analysis strictly assumes the sedimentation of non-interacting particles, and apoE is in an equilibrium, our data suggests that the low mass apoE has a near-homogenous population, most likely to be tetramers or octamers or the equilibrium thereof [23]. For convenience, we will refer to the lower mass apoE as a tetramer.

ApoE4 tetramers aggregate more rapidly than apoE3 and apoE2 tetramers

At 4 ^{o}C, purified apoE tetramers (0.1–1 mg/ml) aggregated only very slowly when stored for approximately 1–2 days as shown by gel filtration chromatography. However, incubation at 37 ^{o}C induced aggregation that differed in rate among the isoforms. Gel filtration chromatography of the tetramer stored at 4 ^{o}C (in 100 mM NH_4HCO_3, pH 7.8 (AB)) resulted in a single peak (Figure 1c). By 4 h of incubation at 37 ^{o}C, apoE4 mostly eluted in the void volume of the column, indicating pronounced self-association into higher molecular mass oligomers (Figure 1c). These aggregates were soluble with no obvious turbidity and did not pellet in a microcentrifuge (×13,000 *g*; 30 min). ApoE3 and apoE2 aggregated far more slowly. Even after 24 h at 37 ^{o}C, most of the apoE2 or apoE3 remained tetrameric (Figure 1c). The rates of aggregation were also slower at lower protein concentrations (0.2 mg/ml), but apoE4 still mostly formed higher mass aggregates within 4 h of incubation (Figure 1d). Similar rates of aggregation were obtained in other buffers (135 mM NaCl, 2.7 mM KCl, 4.3 mM Na_2HPO_4, 1.4 mM KH_2PO_4, pH 7.4 (PBS) and 10 mM Tris, 150 mM NaCl, 0.25 mM EDTA, 0.05% NaN_3, pH 7.4 (TBS)) that also have near-physiological pH and salt concentrations.

ApoE aggregates adopt certain amyloid-like properties but are distinctly unique

To investigate the possibility that apoE forms amyloid fibrils, we first analyzed their morphology by negative staining electron microscopy. ApoE4 aggregates were prepared by incubating the tetramer (0.4 mg/ml) at 37 ^{o}C overnight. The shorter

clearly separated aggregates appeared as semi-regular structures with an average width of 14 ±6 nm and a length of 175 ±35 (Figure 2). These are comparable in width to various amyloid fibrils of other proteins (*e.g.* 2–15 nm) but are somewhat shorter and less regular looking, suggesting a novel structure (Figure 2) [26-28]. The fibrillar morphology of the aggregates did not change for apoE4 incubated at 37 ^{o}C for up to one week. Tetrameric apoE4 did not show any observable feature.

We also tested whether the apoE4 tetramer and aggregated apoE4 bound to two amyloid-binding dyes, thioflavin T and Congo Red. Upon binding to amyloid fibrils formed by many proteins, thioflavin T fluorescence increases [29]. Tetrameric apoE induced an increase in thioflavin T fluorescence emission intensity (Figure 3a). However, after 4 h of incubation at 37 ^{o}C, the same concentrations of apoE4 doubled the fluorescence emission intensity, consistent with a conformational change into an amyloid-like structure (Figure 3a). The excitation spectra monitored by fluorescence emission at 480 nm show a maximum near 280 nm in the presence of apoE, which most likely results from fluorescence resonance energy transfer of the tryptophans of apoE to bound thioflavin T (Figure 3b). This maximum at 280 nm is also about 30% larger apoE4 incubated for 4 h at 37 ^{o}C than tetramer, consistent with more thioflavin T binding to the aggregate than to the tetramer (Figure 3b).

The binding of Congo Red to Aβ amyloid fibrils increases the dye's molar absorptivity and shifts the maximum wavelength from ~490 to 540 nm [30]. When bound to many amyloid fibrils, Congo Red also shows red-green birefringence under cross-polarized light [31]. Incubation of apoE at 37 ^{o}C produced greater changes in the Congo Red absorption spectrum than the tetramer at the same concentrations (Figure 3c), as would be predicted for a change of the tetramer into an amyloid-like aggregate. However, despite binding, Congo Red did not display detectable green birefringence suggesting that the aggregates adopt a novel fibrillar architecture.

Another criterion for amyloid is a rich β-sheet content, comprising the assembly core of the fibrils [32]. To investigate the secondary structure of apoE4 over a time course of aggregation, we used circular dichroism (CD) spectroscopy. The tetramer had a CD spectrum consistent with a high proportion of α-helix, as characterized by the double minima at ~208 and 222 nm (Figure 4a). Incubation of the tetramer at 37 ^{o}C decreased the intensity of the mean residue ellipticity, indicating a loss of α-helical structure and gain of an alternative conformation (Figure 4a). The content of secondary structure of apoE4 at each time point was analysed with the algorithm CONTIN/LL, which fits the experimental data to sets of known crystal structures with their corresponding CD spectra [33-35]. The resulting fits of the CONTIN/LL analysis superimpose the experimental data in Figure 4a. The fractional content of secondary structure derived from the fits show that aggregated apoE4 retained a high proportion of α-helical structure with only modest increases in β-sheet (Figure 4b).

We also tested the apoE4 aggregates for cross-β-sheet structure by x-ray fiber diffraction. Amyloid fibrils have a signature diffraction pattern at 4.7 Å and approximately 9.5 Å that arises from the spacing between β-strands and β-sheets,

respectively, within the fibril core [32]. The diffraction pattern of the apoE4 aggregates had two diffuse rings centered at 4.7 Å and 9–11 Å, in the correct position for β-strand and sheet spacing (Figure 4c). However, the diffraction lacked the sharp meridional and equatorial arcs of highly aligned amyloid, which suggests a less-oriented sample and may reflect the high α-helical structure and unusual morphology.

The rates of aggregation were compared for all three isoforms by thioflavin T reactivity upon incubation of tetramer at 37 ^{o}C (Figure 5). Thioflavin T-reactive material formed in the order, apoE4 > apoE3 > apoE2, consistent with the results of the gel filtration studies. Aggregates of apoE2 and apoE3 were indistinguishable from those of apoE4 by electron microscopy (data not shown). Thus, the three isoforms seem to form aggregates that are of similar structure, but differ in the rate of formation.

ApoE aggregates are more toxic to cultured neuronal cells than tetramer

Increasing evidence suggests that fibrillar and non-fibrillar protein oligomers are inherently toxic to cells relative to the unaggregated forms [36-39]. We tested whether aggregated apoE4 was more toxic than tetramer to a mouse neuronal cell line (Neuro-2a), using propidium iodide reactivity to measure of cell viability. Propidium iodide is excluded from living cells, but intercalates into the DNA of dying cells to produce a highly fluorescent adduct. Aggregated apoE4 was made by pre-incubating the tetramer (0.3 mg/ml) overnight at 37 ^{o}C beforehand. Tetramer or pre-incubated apoE4 was added to the cells at concentrations spanning the range found in brain tissue (~0.01–0.03 mg/ml brain volume) [40].

After a 24-h incubation, viable and non-viable cells were counted by flow cytometry (Figure 6a). Approximately 3% of the untreated control cells were classified as dead (Figure 6b). At comparable concentrations, pre-incubated apoE4 resulted in a greater fraction of dead cells than the tetramer (Figure 6b). It is important to note that while the tetramer itself causes significant toxicity, this may result from pronounced aggregation during the 24-h incubation of the cells at 37 ^{o}C.

To further investigate the isoform dependence on toxicity, we measured the effect of tetrameric and pre-incubated forms of all three isoforms on cell viability using a standard 3-(4,5-dimethylthiazol-2-yl)-2,5-diphenyltetrazolium bromide (MTT) reduction assay, an indicator of mitochondrial functioning. Preincubation of tetrameric apoE (0.3 mg/ml) overnight at 37 ^{o}C resulted in the aggregation of about 5% of apoE2, 10% of apoE3 and 90% of apoE4. For all isoforms, pre-incubated apoE was significantly more toxic than comparable concentrations of tetramer at 0.03 or 0.15 mg/ml (Figure 6d *versus* 6c). In addition, preincubated apoE4 was more toxic than apoE3 and apoE2 at comparable concentrations of protein, consistent with the toxicity correlating to the amount of added aggregate (Figure 6d).

Tetrameric apoE2 was not significantly toxic to the cells at any concentration and apoE3 was toxic only at the highest concentration (0.15 mg/ml). Because tetrameric apoE2 and apoE3 are only likely to aggregate minimally in the cell culture medium during the time span of the experiment, tetrameric apoE likely has little, if any, inherent toxicity.

Conformational stability differences of the isoforms seems to drive aggregation

Previously, we identified two key structural and biophysical differences among the isoforms that are likely to influence the function of apoE [41-43]. One difference is in the interaction between two domains of apoE, known as domain interaction, which is more pronounced in apoE4 than apoE3 and apoE2 [42, 44]. The second is large differences among the isoforms in the conformational stability of the amino-terminal domain [43].

To establish whether domain interaction mediates aggregation, we investigated the aggregation properties of apoE4 in which domain interaction was disrupted by the R61T or the E255A mutations [42]. Either mutation changes the lipoprotein binding preference, a measure of domain interaction, of apoE4 to more closely resemble apoE3 [42].

The E255A mutation did not alter the aggregation properties of apoE4 (Figure 7a). However, in striking contrast, the R61T mutation resulted in greater resistance to aggregation (Figure 7b). Because both mutants disrupt domain interaction yet produce different effects, these results indicate that domain interaction does not explicitly mediate aggregation. One explanation for this result is that Thr-61 modifies the conformational stability of the amino-terminal domain, which substantially differs between the three isoforms [43, 45]. ApoE4 readily forms a molten globule intermediate and is most readily denatured; apoE2 is the most resistant to denaturation, and apoE3 is intermediate [43, 45]. The difference in conformational stability may increase the lipid-binding properties of apoE4 over apoE3 as a result of destabilization of the hydrophobic core [43, 46]. Analogously, a destabilized conformation also could promote misfolding into aggregates, including amyloid fibrils [47].

To investigate this possibility, we determined the guanidine denaturation curves of apoE3, apoE4 and the R61T-apoE4 mutant (Figure 7c). The curves showed biphasic cooperativity, as observed previously for apoE3 and apoE4, reflecting independent folding of the two modular domains [45, 48]. The lower part of the curve represents the unfolding of the carboxyl-terminal domain, which unfolds in the range of 0–1.5 M guanidine hydrochloride; while the upper region of the curve represents the amino-terminal domain, which unfolds in the range of 1.2–4 M guanidine hydrochloride [45]. The R61T-apoE4 mutant displayed an intermediate denaturation curve between apoE3 and apoE4, indicating that the R61T mutation increases the stability of the folded conformation, consistent with the hypothesis that differences in stability are responsible for the differences in aggregation rate (Figure 7c).

To further investigate the effect of conformational stability differences on aggregation, we assessed the aggregation properties of wild-type mouse apoE; the T61R mutant of mouse apoE, which introduces domain interaction [49]; and the T61R, G83T, N113G mutant of mouse apoE, which introduces domain interaction and a substantially reduced conformational stability of the amino-terminal domain [50]. Wild-type mouse apoE and the T61R mutant, like apoE2, have a 2-state-like folding cooperativity and a high midpoint of denaturation [50]. The T61R, G83T, N113G mutant has a lower midpoint of denaturation,

more similar to that of apoE4, and greater ability to remodel phospholipids than the T61R mutant [50]. The purified low mass mouse apoE was monitored for the formation of aggregates. Wild-type mouse apoE and the "domain interaction" derivative, T61R mouse apoE, resisted aggregation as followed by thioflavin T reactivity (Figure 7d). In contrast, the T61R, G83T, N113G mutant rapidly formed thioflavin T-reactive material (Figure 7d). These data further support the hypothesis that stability differences, and not domain interaction, influence aggregation rates.

DISCUSSION

This study shows that apoE4 tetramer has a marked propensity to form toxic, high molecular mass fibrillar oligomers whereas apoE3 and apoE2 tend not.

A unique structure: α-helical apoE fibers?

The high molecular mass aggregates have some properties of amyloid fibrils, including the binding to thioflavin T and Congo Red and a fibrillar morphology, yet differ in having a high α-helical content, fibrils of less regular shape, and a lack of Congo Red red-green birefringence. Our conclusions are similar to that of a study of the yeast prion protein, Ure2p, which has many amyloid-like properties, but forms enzymatically active aggregates with α-helical structure, which suggests that α-helical aggregates may be prevalent in some amyloid-related diseases [51].

An intriguing possibility is that apoE4 forms a protofilament-type β-sheet core stabilized by only a few residues, with extraneous regions remaining highly α-helical. Such a structure would account for the observed discrepancies with the classic properties of amyloid-fibrils (Figure 8a). Alternatively, apoE aggregates may be stabilized solely by helix–helix interactions (Figure 8b) or by a combination of β-strand and helix–helix interactions. Several lines of evidence support a role for the involvement of supramolecular α-helices in aggregate stabilization. One is a recent study suggesting that the carboxyl-terminal domain of apoE forms coiled–coil oligomers, which is a common structural motif for fibers [52]. The morphology of the apoE4 aggregates (Figure 4), is also similar to coiled-coil fibers of the intermediate filament protein vimentin, to fibers of the engineered domain-swapped protein DSAg, and to fibers of the plant protein remorin [53-55].

Insight is also gained by consideration of the structural properties of apoA-II and apoA-I. Different structures of apoA-I and apoA-II reveal significant structural plasticity in the supramolecular assembly of helices [56-58]. For example, lipid-free apoA-II forms stacks of linear α-helices, whereas detergent-bound apoA-II forms a looped fiber of curved double-stranded helices [57]. A fragment of apoA-I (residues 44–243) forms an elliptical ring-like tetramer of interacting α-helices [56]. This contrasts to full length apoA-I where the helices are configured completely differently [58]. In this structure, apoA-I has a conformation strikingly similar to that of apoE with a four-helix amino-terminal domain separated by a linker and two

carboxyl-terminal helices [58]. These data highlight the similarities in structure and function in lipoprotein metabolism of apoE and apoA-I and point to the potential for apoE aggregates being stabilized by extended helix–helix interactions.

Conformational flexibility of the apolipoproteins and their propensity for misfolding and amyloid fibril association

Other proteins with amphipathic α-helices that mediate reversible lipid-binding, a characteristic property of the exchangeable apolipoprotein family, also readily form amyloid fibrils *in vitro* or *in vivo* [27]. In particular, apoA-I, apoA-II, and serum amyloid A, and mutants thereof are associated with many forms of amyloidoses, and apoC-II forms amyloid fibrils *in vitro* [20, 59].

In the lipid-free form, many apolipoproteins have lipid-binding domains of low conformational stability or are natively unfolded [20, 60]. A marginal conformational stability may provide flexibility by facilitating the dynamic sampling of different conformations that have different lipid–protein or protein–protein affinities [20]. However, destabilizing the native globular fold can also promote amyloid and aggregate formation [47]. Amphipathic α-helical structure is stabilized upon lipid binding, which may protect the protein from amyloidogenic folding pathways (Figure 8). The completely different helical arrangements of the two crystal structures of apoA-I suggest a high degree of conformational flexibility, which may reflect its ability to reversibly bind lipoprotein particles [56, 58]. Accumulating evidence suggests that apoE, like apoA-I, is highly conformationally adaptable [44, 61-65].

The association of apoE with amyloid-related diseases

ApoE is found in almost all type of amyloid plaques, plays a major role in the risk of Alzheimer's disease, and modulates Aβ plaque pathology in mouse models of Alzheimer's disease [1, 6, 15-19]. Could apoE aggregation be a key component of protein aggregation pathways in amyloid-related diseases? The ability of apoE4 to form neurotoxic aggregates more readily than apoE3 or apoE2 casts a new light on the pathological role of apoE. The aggregates could behave in a toxic manner similar to that of soluble aggregates of Aβ or other aggregation-prone proteins in the brains of Alzheimer's patients [38, 39, 66]. The apoE aggregates could also nucleate Aβ aggregation or plaque formation. In support of this concept, other studies have shown the binding/colocalization of apoE4 and Aβ, modulation of Aβ fibril morphology by apoE4 *in vitro*, and promotion of amyloid plaque deposition by apoE *in vivo* [15, 16, 18, 67, 68]. Additional insight comes from recent studies on ABCA-1 knockout mice, in which the absence of ABCA-1 results in the secretion of poorly-lipidated apoE from astrocytes [69, 70]. ABCA-1 knockout mice crossed to transgenic mouse lines that also overproduce Aβ results in greatly enhanced amyloid plaque deposition [71-73]. This result is consistent with the hypothesis that lipid-poor pools of apoE in the brain can aggregate, stimulating Aβ aggregation and deposition.

The formation of apoE fibrils *in vivo* may require the presence of lipid-free or lipid-poor reservoirs of apoE, since lipid-binding likely protects apolipoproteins from misfolding into amyloid fibrils [20] (Figure 8). ApoE has been mostly characterized when bound to lipoproteins from plasma and cerebrospinal fluid (CSF). However, there is evidence for other discrete pools of apoE. Lipid-poor forms of apoE exist in plasma [74], in the extracellular matrix of hepatic cells [75], and when secreted by or cell-surface bound to macrophages in the absence of an exogenous cholesterol source [76, 77]. In the brain most apoE is not in the CSF [40, 78]. This non-CSF apoE is distributed widely throughout the brain and is mostly localized to astrocytes and in distinct intracellular and extracellular locations [40]. This leaves open the potential for lipid-free apoE reservoirs that are vulnerable to aggregation and hence association with amyloid plaques.

In conclusion, our findings that apoE forms fibrillar aggregates in physiological buffers, which are toxic to neuronal cells, suggest that apoE may play a direct toxic role in diseases such as Alzheimer's through a novel mechanism. That apoE4 forms fibrils significantly faster than apoE3 and apoE2, provides a striking and novel correlation with the risk these isoforms convey to neurological disease.

MATERIALS AND METHODS

Protein purification, refolding and isolation of homogenous apoE tetramer

ApoE was expressed in *E. coli* and purified as described with modifications [44, 79]. Mutations were made directly in the expression vector with the QuickChange XL mutagenesis kit (Novagen), and the sequences were verified by DNA sequencing.

Homogeneous populations of apoE were isolated as described [44]. Briefly, apoE was refolded from a 4 M guanidine hydrochloride stock by injecting stock protein onto a Superdex 200 gel filtration column equilibrated in PBS, TBS or AB. The protein eluted as two peaks. The first peak represented high mass material, likely to be misfolded or aggregated protein. The second peak, corresponding to lower mass apoE, was collected and stored at 4 ^{o}C for up to 24 h, or snap-frozen in liquid nitrogen and stored at –80 ^{o}C for longer storage. As assessed by gel filtration chromatography, snap-frozen apoE had no change in aggregation state when thawed. Because the destabilized T61R, G83T, N113G mouse apoE derivative aggregated much faster than the other mouse and human apoE variants, all mouse apoE samples were stored snap frozen in aliquots for time-course experiments.

Sedimentation velocity analysis

ApoE4 (0.5 mg/ml) in TBS was analyzed with an XL-A analytical ultracentrifuge (Beckman Coulter, Fullerton, CA) in an AnTi60 rotor. A sample volume of 400 μl was used, and radial scans were recorded at 10-min intervals at the angular velocity of 30,000 rpm. Data were analysed with the vHW method and a continuous size distribution, $c(s)$, using the software SEDFIT [24, 25]. For $c(s)$ analysis, a regularization parameter of p = 0.95, and resolution of 100 sedimentation coefficient increments were used in the fitting in the range 1–20 S, and the best fit frictional ratio (f/f_0) of 2.1 was found using non–linear regression analysis in the software. A partial specific volume of 0.73 ml/g was calculated from the amino acid compositions of apoE and a buffer density of 1.043 g/ml was used in the calculations.

Analytical gel filtration chromatography

Samples of apoE in AB with 10 mM DTT were incubated at 37 ^{o}C. Aliquots (500 μl) were subjected to gel filtration chromatography on a Superdex 200 10/300 GL column (Pharmacia) pre-equilibrated with buffer TBS and run at a flow rate of 0.5 ml/min.

Thioflavin T fluorescence spectroscopy

For the spectral analysis of apoE4, tetramer was prepared at 0.4 mg/ml in TBS and samples were incubated at 37 ^{o}C for various times. Emission spectra (excitation at 445 nm) were collected for thioflavin T (5 μM) and apoE4 (20–100 μg/ml) at

room temperature with a Perkin-Elmer LS-5B luminescence spectrometer. Excitation spectra were collected using an emission wavelength of 480 nm. Excitation and emission bandwidths of 5 nm and 10 nm, respectively, were used.

For the time-course experiments, 80–100-μl samples of tetrameric apoE (0.4–0.6 mg/ml) in TBS and 0.5 mM tris-(2-carboxyethyl)phosphine were incubated at 37 °C with a heated-top PCR thermocycler. Thioflavin T was added to the tubes to a final volume of 250 μl and Thioflavin T concentration of 5 μM. 200 μl of the resulting solution was analyzed in a fluorescence plate reader (Molecular Devices FlexStation II with an excitation wavelength of 420 nm, an emission wavelength of 480 nm, and an emission filter of 435 nm).

Congo Red binding

ApoE4 tetramer was prepared at 0.4 mg/ml in TBS and incubated at 37 °C for various times. The absorbance spectrum of apoE4 (100 μg/ml) with Congo Red (3.75 μM) in TBS was monitored with a Beckman Du-450 spectrophotometer. For detection of red-green birefringence, apoE4 aggregates were collected by high-speed spins (30 min, 100,000 rpm in a Beckman TLA 100.2 rotor), and the pelleted protein was stained and visualized as described [27].

Transmission electron microscopy

ApoE (0.1–0.5 mg/ml) in TBS or PBS was applied to a carbon-coated grid for 30 sec and negatively stained with 2% sodium phosphotungstate, pH 7.4, for 30 sec. Samples were imaged in a Siemans Elmiskop 101 electron microscope at magnifications of ×10,000–×60,000. Fibril dimensions were measured with the segmented line tool in the ImageJ version 1.34s software [80].

Circular dichroism spectroscopy

ApoE4 tetramer (0.15 mg/ml) was prepared in PBS and incubated at 37 °C for various times. Spectra were collected at 20 °C in a 1-mm pathlength cuvette. Ten scans were collected and averaged with a Jasco J-710 spectropolarimeter using a bandwidth of 2 nm and a data pitch of 0.1 nm. Data were also analyzed using the software suite CDpro and with the 56-protein reference set [33-35].

X-ray fiber diffraction

ApoE4 (0.4 mg/ml) tetramer in AB was incubated overnight at 37 °C and then concentrated to ~20 mg/ml with a Speedvac. The concentrated protein was dried in an x-ray crystallographic glass capillary at room temperature. X-ray diffraction data were collected on a Rigaku rotating anode generator fitted with Osmic "blue" mirrors and an R-axis IV detector using CuKα radiation. The sample-to-detector distance was 250 mm, and the exposure time 20 min.

Guanidine hydrochloride denaturation curves

ApoE (0.5 mg/mL) in 0–5 M guanidine hydrochloride, 5 mM DTT and 20 mM sodium phosphate, pH 7.4, was pre-incubated overnight at 4 ^{o}C. CD measurements at a wavelength of 222 nm were made on an Applied Biophysics π-180 spectropolarimeter using a 1-mm pathlength cuvette at 25 ^{o}C. Data were standardized to unfolded fractions, assuming that 5 M guanidine hydrochloride completely unfolds apoE.

Neuronal toxicity assays

Neuro-2a cells (American Type Culture Collection, Manassas, VA) were maintained at 37 °C in a humidified 5% CO_2 incubator in MEM containing 10% FBS supplemented with nonessential amino acids, penicillin, and streptomycin. Cells were plated at a density of 10,000 cells per well on 96-well plates in 100 μl of fresh medium (for the MTT reduction assay) or 30,000 cells per well on 24-well plates in 500 μl medium (for flow cytometry). ApoE was added to the cell medium at a final apoE concentration of 0, 0.003, 0.03 or 0.15 mg/ml and a 1:1 dilution of the medium with PBS, and the cells were incubated for 24 h before assessment of cell viability. For the MTT reduction assay, 10 μl of MTT (5 mg/ml in PBS) was added to the medium, and the cells were incubated for 4 h. Cells were lysed with 20% SDS, 50% N,N-dimethylformamide, pH 4.7 (100 μl), and incubated overnight at 37 °C in an humidified incubator. The development of blue formazan (MTT reduction) was measured by absorbance spectrometry at 590 nm. For flow cytometry, cells were trypsinized, washed in PBS, and resuspended in 1 ml of PBS. Propidium iodide (2 mg/ml, 1 μl) was added to each sample and incubated for 5 min on ice. Cells were counted with a FACSCaliburs P2 (BD Biosciences) flow cytometer using an excitation wavelength of 488 nm and emission wavelength of 550 nm.

ACKNOWLEDGEMENTS

We thank Jinny Wong, Jo Dee Fish, Maryam Tabar and Maya Mathew for technical assistance, Louise Serpell, Sumner Makin and Robert Stroud for helpful comments, Stephen Ordway and Gary Howard for editorial assistance, John Carroll, Jack Hull, Steven Gonzales and Chris Goodfellow for graphics assistance, and Karina Fantillo for manuscript preparation. This work was supported in part by grants from the National Institutes of Health P01 AG022074, R01 AG020235 and a postdoctoral fellowship to D.M.H. from the John Douglas French Alzheimer's Foundation.

REFERENCES

1. Farrer, L. A., Cupples, L. A., Haines, J. L., Hyman, B., Kukull, W. A., Mayeux, R., *et al.* (1997) Effects of age, sex, and ethnicity on the association between apolipoprotein E genotype and Alzheimer disease. A meta-analysis. *J. Am. Med. Assoc.*, **278**, 1349–1356.
2. Weisgraber, K. H., Rall, S. C., Jr. & Mahley, R. W. (1981) Human E apoprotein heterogeneity. Cysteine-arginine interchanges in the amino acid sequence of the apo-E isoforms. *J. Biol. Chem.*, **256**, 9077–9083.
3. Strittmatter, W., Weisgraber, K., Huang, D., Dong, L., Salvesen, G., Pericak-Vance, M., *et al.* (1993) Binding of human apolipoprotein E to synthetic amyloid β- peptide: Isoform-specific effects and implications for late-onset Alzheimer disease. *Proc. Natl. Acad. Sci. USA*, **90**, 8098-8102.
4. Nicoll, J. A. R., Roberts, G. W. & Graham, D. I. (1995) Apolipoprotein E ε4 allele is associated with deposition of amyloid β-protein following head injury. *Nat. Med.*, **1**, 135–137.
5. Buttini, M., Orth, M., Bellosta, S., Akeefe, H., Pitas, R. E., Wyss-Coray, T., *et al.* (1999) Expression of human apolipoprotein E3 or E4 in the brains of *Apoe*$^{-/-}$ mice: Isoform-specific effects on neurodegeneration. *J. Neurosci.*, **19**, 4867–4880.
6. Holtzman, D. M., Bales, K. R., Tenkova, T., Fagan, A. M., Parsadanian, M., Sartorius, L. J., *et al.* (2000) Apolipoprotein E isoform-dependent amyloid deposition and neuritic degeneration in a mouse model of Alzheimer's disease. *Proc. Natl. Acad. Sci. USA*, **97**, 2892–2897.
7. Huang, Y., Liu, X. Q., Wyss-Coray, T., Brecht, W. J., Sanan, D. A. & Mahley, R. W. (2001) Apolipoprotein E fragments present in Alzheimer's disease brains induce neurofibrillary tangle-like intracellular inclusions in neurons. *Proc. Natl. Acad. Sci. USA*, **98**, 8838-8843.
8. Ji, Z.-S., Miranda, R. D., Newhouse, Y. M., Weisgraber, K. H., Huang, Y. & Mahley, R. W. (2002) Apolipoprotein E4 potentiates amyloid β peptide-induced lysosomal leakage and apoptosis in neuronal cells. *J. Biol. Chem.*, **277**, 21821–21828.
9. Harris, F. M., Brecht, W. J., Xu, Q., Tesseur, I., Kekonius, L., Wyss-Coray, T., *et al.* (2003) Carboxyl-terminal-truncated apolipoprotein E4 causes Alzheimer's disease-like neurodegeneration and behavioral deficits in transgenic mice. *Proc. Natl. Acad. Sci. USA*, **100**, 10966-10971.
10. Marques, M. A. & Crutcher, K. A. (2003) Apolipoprotein E-related neurotoxicity as a therapeutic target for Alzheimer's disease. *J. Mol. Neurosci.*, **20**, 327-337.
11. Dolev, I. & Michaelson, D. M. (2004) A nontransgenic mouse model shows inducible amyloid-β (Aβ) peptide deposition and elucidates the role of apolipoprotein E in the amyloid cascade. *Proc. Natl. Acad. Sci. USA*, **101**, 13909–13914.
12. Schmechel, D., Saunders, A., Strittmatter, W., Crain, B., Hulette, C., Joo, S., *et al.* (1993) Increased amyloid β-peptide deposition in cerebral cortex as a consequence of apolipoprotein E genotype in late-onset Alzheimer disease. *Proc. Natl. Acad. Sci. USA*, **90**, 9649-9653.
13. Wisniewski, T., Lalowski, M., Golabek, A., Vogel, T. & Frangione, B. (1995) Is Alzheimer's disease an apolipoprotein E amyloidosis? *Lancet*, **345**, 956–958.
14. Cho, H. S., Hyman, B. T., Greenberg, S. M. & Rebeck, G. W. (2001) Quantitation of apoE domains in Alzheimer disease brain suggests a role for apoE in Aβ aggregation. *J. Neuropathol. Exp. Neurol.*, **60**, 342-349.
15. Namba, Y., Tomonaga, M., Kawasaki, H., Otomo, E. & Ikeda, K. (1991) Apolipoprotein E immunoreactivity in cerebral amyloid deposits and neurofibrillary tangles in Alzheimer's disease and kuru plaque amyloid in Creutzfeldt–Jakob disease. *Brain Res.*, **541**, 163–166.
16. Wisniewski, T. & Frangione, B. (1992) Apolipoprotein E: A pathological chaperone protein in patients with cerebral and systemic amyloid. *Neurosci. Lett.*, **135**, 235–238.

17. Sheng, J. G., Mrak, R. E. & Griffin, W. S. (1996) Apolipoprotein E distribution among different plaque types in Alzheimer's disease: Implications for its role in plaque progression. *Neuropathol. Appl. Neurobiol.*, **22**, 334–341.
18. Naidu, A., Catalano, R., Bales, K., Wu, S., Paul, S. M. & Cordell, B. (2001) Conversion of brain apolipoprotein E to an insoluble form in a mouse model of Alzheimer disease. *Neuroreport,* **12**, 1265–1270.
19. Matsutani, H., Hoshii, Y., Setoguchi, M., Kawano, H., Gondo, T., Takahashi, M., *et al.* (2001) Vascular amyloid of unknown origin and senile transthyretin amyloid in the lung and gastrointestinal tract of old age: Histological and immunohistochemical studies. *Path. Int.*, **51**, 326-332.
20. Hatters, D. M. & Howlett, G. J. (2002) The structural basis for amyloid formation by plasma apolipoproteins: A review. *Eur. Biophys. J.*, **31**, 2–8.
21. Aggerbeck, L. P., Wetterau, J. R., Weisgraber, K. H., Wu, C.-S. C. & Lindgren, F. T. (1988) Human apolipoprotein E3 in aqueous solution. II. Properties of the amino- and carboxyl-terminal domains. *J. Biol. Chem.*, **263**, 6249–6258.
22. Yokoyama, S., Kawai, Y., Tajima, S. & Yamamoto, A. (1985) Behavior of human apolipoprotein E in aqueous solutions and at interfaces. *J. Biol. Chem.*, **260**, 16375–16382.
23. Perugini, M. A., Schuck, P. & Howlett, G. J. (2000) Self-association of Human Apolipoprotein E3 and E4 in the Presence and Absence of Phospholipid. *J. Biol. Chem.*, **275**, 36758-36765.
24. Van Holde, K. E. & Weischet, W. O. (1978) Boundary analysis of sedimentation-velocity experiments with monodisperse and paucidisperse solutes. *Biopolymers*, **17**, 1387-1403.
25. Schuck, P. (2000) Size-Distribution Analysis of Macromolecules by Sedimentation Velocity Ultracentrifugation and Lamm Equation Modeling. *Biophys. J.*, **78**, 1606-1619.
26. Chamberlain, A. K., MacPhee, C. E., Zurdo, J., Morozova-Roche, L. A., Hill, H. A. O., Dobson, C. M., *et al.* (2000) Ultrastructural organization of amyloid fibrils by atomic force microscopy. *Biophys. J.*, **79**, 3282–3293.
27. Hatters, D. M., MacPhee, C. E., Lawrence, L. J., Sawyer, W. H. & Howlett, G. J. (2000) Human Apolipoprotein C-II Forms Twisted Amyloid Ribbons and Closed Loops. *Biochemistry,* **39**, 8276-8283.
28. Goldsbury, C. S., Cooper, G. J. S., Goldie, K. N., Müller, S. A., Saafi, E. L., Gruijters, W. T. M., *et al.* (1997) Polymorphic fibrillar assembly of human amylin. *J. Struct. Biol.*, **119**, 17–27.
29. LeVine, H., 3rd (1999) Quantification of β-sheet amyloid fibril structures with thioflavin T. *Methods Enzymol.*, **309**, 274-284.
30. Klunk, W. E., Jacob, R. F. & Mason, R. P. (1999) Quantifying amyloid β-peptide (Aβ) aggregation using the Congo Red-Aβ (CR-Aβ) spectrophotometric assay. *Anal. Biochem.*, **266**, 66-76.
31. Nilsson, M. R. (2004) Techniques to study amyloid fibril formation *in vitro*. *Methods*, **34**, 151-160.
32. Sunde, M., Serpell, L. C., Bartlam, M., Fraser, P. E., Pepys, M. B. & Blake, C. C. F. (1997) Common core structure of amyloid fibrils by synchrotron X-ray diffraction. *J. Mol. Biol.*, **273**, 729-739.
33. Provencher, S. W. & Glöckner, J. (1981) Estimation of globular protein secondary structure from circular dichroism. *Biochemistry,* **20**, 33–37.
34. Johnson, W. C. (1999) Analyzing protein circular dichroism spectra for accurate secondary structures. *Proteins*, **35**, 307–312.
35. Sreerama, N. & Woody, R. W. (2000) Estimation of protein secondary structure from circular dichroism spectra: Comparison of CONTIN, SELCON, and CDSSTR methods with an expanded reference set. *Anal. Biochem.*, **287**, 252–260.

36. Mendes Sousa, M., Cardoso, I., Fernandes, R., Guimaraes, A. & Saraiva, M. J. (2001) Deposition of transthyretin in early stages of familial amyloidotic polyneuropathy: Evidence for toxicity of nonfibrillar aggregates. *Am. J. Pathol.*, **159**, 1993-2000.
37. Walsh, D. M., Klyubin, I., Fadeeva, J. V., Cullen, W. K., Anwyl, R., Wolfe, M. S., *et al.* (2002) Naturally secreted oligomers of amyloid β-protein potently inhibit hippocampal long-term potentiation *in vivo*. *Nature*, **416**, 535-539.
38. Bucciantini, M., Giannoni, E., Chiti, F., Baroni, F., Formigli, L., Zurdo, J., *et al.* (2002) Inherent toxicity of aggregates implies a common mechanism for protein misfolding diseases. *Nature*, **416**, 507–511.
39. Kayed, R., Head, E., Thompson, J. L., McIntire, T. M., Milton, S. C., Cotman, C. W., *et al.* (2003) Common structure of soluble amyloid oligomers implies common mechanism of pathogenesis. *Science*, **300**, 486–489.
40. Boyles, J. K., Pitas, R. E., Wilson, E., Mahley, R. W. & Taylor, J. M. (1985) Apolipoprotein E associated with astrocytic glia of the central nervous system and with nonmyelinating glia of the peripheral nervous system. *J. Clin. Invest.*, **76**, 1501–1513.
41. Weisgraber, K. H. & Mahley, R. W. (1996) Human apolipoprotein E: The Alzheimer's disease connection. *FASEB J.*, **10**, 1485–1494.
42. Dong, L.-M. & Weisgraber, K. H. (1996) Human apolipoprotein E4 domain interaction. Arginine 61 and glutamic acid 255 interact to direct the preference for very low density lipoproteins. *J. Biol. Chem.*, **271**, 19053–19057.
43. Morrow, J. A., Hatters, D. M., Lu, B., Höchtl, P., Oberg, K. A., Rupp, B., *et al.* (2002) Apolipoprotein E4 forms a molten globule: A potential basis for its association with disease. *J. Biol. Chem.*, **277**, 50380–50385.
44. Hatters, D. M., Budamagunta, M. S., Voss, J. C. & Weisgraber, K. H. (2005) Modulation of apolipoprotein E structure by domain interaction: Differences in lipid-bound and lipid-free forms. *J. Biol. Chem.*, (in press).
45. Morrow, J. A., Segall, M. L., Lund-Katz, S., Phillips, M. C., Knapp, M., Rupp, B., *et al.* (2000) Differences in stability among the human apolipoprotein E isoforms determined by the amino-terminal domain. *Biochemistry*, **39**, 11657-11666.
46. Weers, P. M. M., Narayanaswami, V., Choy, N., Luty, R., Hicks, L., Kay, C. M., *et al.* (2003) Lipid binding ability of human apolipoprotein E N-terminal domain isoforms: Correlation with protein stability? *Biophys. Chem.*, **100**, 481–492.
47. Dobson, C. M. (2003) Protein folding and misfolding. *Nature*, **426**, 884-890.
48. Wetterau, J. R., Aggerbeck, L. P., Rall, S. C., Jr. & Weisgraber, K. H. (1988) Human apolipoprotein E3 in aqueous solution. I. Evidence for two structural domains. *J. Biol. Chem.*, **263**, 6240–6248.
49. Raffai, R. L., Dong, L.-M., Farese, R. V., Jr. & Weisgraber, K. H. (2001) Introduction of human apolipoprotein E4 "domain interaction" into mouse apolipoprotein E. *Proc. Natl. Acad. Sci. USA*, **98**, 11587-11591.
50. Hatters, D. M., Peters-Libeu, C. A. & Weisgraber, K. H. (2005) Engineering Conformational Destabilization into Mouse Apolipoprotein E: A model for a unique property of human apolipoprotein E4. *J. Biol. Chem.*, **280**, 26477-26482.
51. Bousset, L., Thomson, N. H., Radford, S. E. & Melki, R. (2002) The yeast prion Ure2p retains its native α-helical conformation upon assembly into protein fibrils *in vitro*. *EMBO J.*, **21**, 2903-2911.
52. Choy, N., Raussens, V. & Narayanaswami, V. (2003) Inter-molecular coiled-coil formation in human apolipoprotein E C-terminal domain. *J. Mol. Biol.*, **334**, 527-539.

53. Ogihara, N. L., Ghirlanda, G., Bryson, J. W., Gingery, M., DeGrado, W. F. & Eisenberg, D. (2001) Design of three-dimensional domain-swapped dimers and fibrous oligomers. *Proc. Natl. Acad. Sci. USA*, **98**, 1404-1409.
54. Bariola, P., Retelska, D., Stasiak, A., Kammerer, R., Fleming, A., Hijri, M., *et al.* (2004) Remorins form a novel family of coiled coil-forming oligomeric and filamentous proteins associated with apical, vascular and embryonic tissues in plants. *Plant Mol. Biol.*, **55**, 579-594.
55. Mucke, N., Wedig, T., Burer, A., Marekov, L. N., Steinert, P. M., Langowski, J., *et al.* (2004) Molecular and biophysical characterization of assembly-starter units of human vimentin. *J. Mol. Biol.*, **340**, 97-114.
56. Borhani, D. W., Rogers, D. P., Engler, J. A. & Brouillette, C. G. (1997) Crystal structure of truncated human apolipoprotein A-I suggests a lipid-bound conformation. *Proc. Natl. Acad. Sci. USA*, **94**, 12291–12296.
57. Kumar, M. S., Carson, M., Hussain, M. M. & Murthy, H. M. K. (2002) Structures of apolipoprotein A-II and a lipid–surrogate complex provide insights into apolipoprotein–lipid interactions. *Biochemistry*, **41**, 11681–11691.
58. Ajees, A. A., Anantharamaiah, G. M., Mishra, V. K., Hussain, M. M. & Murthy, H. M. K. (2006) Crystal structure of human apolipoprotein A-I: Insights into its protective effect against cardiovascular diseases. *Proc. Natl. Acad. Sci. USA*, **103**, 2126-2131.
59. Sorci-Thomas, M. G. & Thomas, M. J. (2002) The Effects of Altered Apolipoprotein A-I Structure on Plasma HDL Concentration. *Trends Cardiovasc. Med.*, **12**, 121-128.
60. Gursky, O. (2005) Apolipoprotein structure and dynamics. *Curr. Opin. Lipidol.*, **16**, 287-294.
61. Raussens, V., Fisher, C. A., Goormaghtigh, E., Ryan, R. O. & Ruysschaert, J.-M. (1998) The low density lipoprotein receptor active conformation of apolipoprotein E. Helix organization in N-terminal domain-phospholipid disc particles. *J. Biol. Chem.*, **273**, 25825–25830.
62. Fisher, C. A. & Ryan, R. O. (1999) Lipid binding-induced conformational changes in the N-terminal domain of human apolipoprotein E. *J. Lipid Res.*, **40**, 93–99.
63. Lu, B., Morrow, J. A. & Weisgraber, K. H. (2000) Conformational reorganization of the four-helix bundle of human apolipoprotein E in binding to phospholipid. *J. Biol. Chem.*, **275**, 20775–20781.
64. Narayanaswami, V., Szeto, S. S. W. & Ryan, R. O. (2001) Lipid association-induced N- and C-terminal domain reorganization in human apolipoprotein E3. *J. Biol. Chem.*, **276**, 37853–37860.
65. Peters-Libeu, C. A., Newhouse, Y., Hatters, D. M. & Weisgraber, K. H. (2006) Model of biologically active apolipoprotein E bound to dipalmitoylphosphatidylcholine. *J. Biol. Chem.*, **281**, 1073-1079.
66. Lambert, M. P., Barlow, A. K., Chromy, B. A., Edwards, C., Freed, R., Liosatos, M., *et al.* (1998) Diffusible, nonfibrillar ligands derived from $A\beta_{1-42}$ are potent central nervous system neurotoxins. *Proc. Natl. Acad. Sci. USA*, **95**, 6448–6453.
67. Sanan, D. A., Weisgraber, K. H., Russell, S. J., Mahley, R. W., Huang, D., Saunders, A., *et al.* (1994) Apolipoprotein E associates with β amyloid peptide of Alzheimer's disease to form novel monofibrils. Isoform apoE4 associates more efficiently than apoE3. *J. Clin. Invest.*, **94**, 860–869.
68. Ma, J., Yee, A., Brewer, H. B., Das, S. & Potter, H. (1994) Amyloid-associated proteins α1-antichymotrypsin and apolipoprotein E promote assembly of Alzheimer β-protein into filaments. *Nature*, **372**, 92-94.
69. Wahrle, S. E., Jiang, H., Parsadanian, M., Legleiter, J., Han, X., Fryer, J. D., *et al.* (2004) ABCA1 Is Required for Normal Central Nervous System ApoE Levels and for Lipidation of Astrocyte-secreted apoE. *J. Biol. Chem.*, **279**, 40987-40993.
70. Hirsch-Reinshagen, V., Zhou, S., Burgess, B. L., Bernier, L., McIsaac, S. A., Chan, J. Y., *et al.* (2004) Deficiency of ABCA1 Impairs Apolipoprotein E Metabolism in Brain. *J. Biol. Chem.*, **279**, 41197-41207.

71. Hirsch-Reinshagen, V., Maia, L. F., Burgess, B. L., Blain, J.-F., Naus, K. E., McIsaac, S. A., *et al.* (2005) The absence of ABCA1 decreases soluble apoE levels but does not diminish amyloid deposition in two murine models of Alzheimer's disease. *J. Biol. Chem.*, **280**, 43243-43256.
72. Koldamova, R., Staufenbiel, M. & Lefterov, I. (2005) Lack of ABCA1 considerably decreases brain ApoE level and increases amyloid deposition in APP23 mice. *J. Biol. Chem.*, **280**, 43224-43235.
73. Wahrle, S. E., Jiang, H., Parsadanian, M., Hartman, R. E., Bales, K. R., Paul, S. M., *et al.* (2005) Deletion of ABCA1 increases Aβ deposition in the PDAPP transgenic mouse model of Alzheimer's disease. *J. Biol. Chem.*, **280**, 43236-43242.
74. Huang, Y., von Eckardstein, A., Wu, S., Maeda, N. & Assmann, G. (1994) A plasma lipoprotein containing only apolipoprotein E and with γ mobility on electrophoresis releases cholesterol from cells. *Proc. Natl. Acad. Sci. USA*, **91**, 1834–1838.
75. Burgess, J. W., Gould, D. R. & Marcel, Y. L. (1998) The HepG2 extracellular matrix contains separate heparinase- and lipid-releasable pools of apoE. *J. Biol. Chem.*, **273**, 5645–5654.
76. Zhang, W.-Y., Gaynor, P. M. & Kruth, H. S. (1996) Apolipoprotein E produced by human monocyte-derived macrophages mediates cholesterol efflux that occurs in the absence of added cholesterol acceptors. *J. Biol. Chem.*, **271**, 28641–28646.
77. Lin, C.-Y., Huang, Z. H. & Mazzone, T. (2001) Interaction with proteoglycans enhances the sterol efflux produced by endogenous expression of macrophage apoE. *J. Lipid Res.*, **42**, 1125–1133.
78. Fagan, A. M., Younkin, L. H., Morris, J. C., Fryer, J. D., Cole, T. G., Younkin, S. G., *et al.* (2000) Differences in the Aβ40/Aβ42 ratio associated with cerebrospinal fluid lipoproteins as a function of apolipoprotein E genotype. *Ann. Neurol.*, **48**, 201–210.
79. Morrow, J. A., Arnold, K. S. & Weisgraber, K. H. (1999) Functional characterization of apolipoprotein E isoforms overexpressed in *Escherichia coli*. *Protein Expr. Purif.*, **16**, 224–230.
80. Abramoff, M. D., Magelhaes, P. J. & Ram, S. J. (2004) Image processing with ImageJ. *Biophotonics International*, **11**, 36-42.

Figure legends

Figure 1. Isoform differences in the rates of self-association of apoE tetramer into aggregates. (a). Sedimentation velocity analysis of low mass apoE. A subset of the analysed sedimenting boundaries are shown at 20-min intervals (gray lines). Data are overlayed with the numerical fits to a *c*(*s*) sedimentation distribution (black dashed lines). **(b).** The obtained *c*(*s*) sedimentation coefficient distribution (black line, left axis) is overlayed with the sedimentation values obtained with the van-Holde Weischet analysis of the same data (open circles, right axis). **(c).** Purified apoE tetramer (0.5 mg/ml) was incubated at 37 ^{o}C in AB buffer, and aliquots were analyzed by gel filtration chromatography at the indicated timepoints. **(d).** Same experiment as panel (c) but with a lower protein concentration (0.2 mg/ml). Comparable results were observed in PBS and TBS buffers for the data in panels (c) and (d).

Figure 2. ApoE4 aggregates have a fibrillar morphology. Transmission electron micrographs of apoE4 aggregates negatively stained with phosphotungstic acid reveal twisted fibrillar structures. ×20,000 magnification.

Figure 3. Differences in apoE4 tetramer and aggregate binding to the amyloid dyes, thioflavin T and Congo Red. (a). Thioflavin T fluorescence emission spectra (5 μM) in presence of 100 μg/ml apoE4 tetramer incubated at 37 ^{o}C for the indicated times. Excitation wavelength was 445 nm. The inset shows a titration of tetramer, 4-h incubated apoE and BSA to a fixed thioflavin T concentration (5 μM). **(b).** Thioflavin T excitation spectra (5 μM) of 100 μg/ml apoE tetramer incubated at 37 ^{o}C for the indicated times, with emission monitored at a wavelength of 480 nm. **(c).** Congo Red absorption spectra (3.75 μM) in the presence of 100 μg/ml apoE4 tetramer incubated at 37 ^{o}C for the indicated times.

Figure 4. Differences in secondary structure between apoE4 tetramer and aggregate. (a). CD spectra of apoE4 tetramers incubated at 37 ^{o}C for the indicated times. Symbols represent experimental data, and lines are the best fit to the CONTIN/LL algorithm, which models the secondary structure content. **(b).** Change in fractional secondary structure of the apoE4 upon incubation at 37 ^{o}C as derived from fits to the CONTIN/LL algorithm. **(c).** X-ray fiber diffraction analysis of apoE4 aggregates. The diffraction rings centered at 4.7 Å and 9–11 Å are characteristic of that for cross-β-sheet in amyloid fibrils.

Figure 5. Isoform-specific differences in the rate of thioflavin T reactivity. Purified apoE tetramer was assessed for changes in thioflavin T reactivity upon incubation at 37 ^{o}C. Each point represents the mean and standard deviation of three independently incubated samples.

Figure 6. ApoE aggregates are more toxic than tetramers to cultured neuronal (Neuro-2a) cells. (a). Histogram of the live and dead Neuro-2a cell populations 24 h after the addition of pre-incubated apoE4, as compared to untreated cells. Data show live/dead Neuro-2a cell count by flow cytometry and propidium iodide fluorescence. **(b).** Percentage of dead Neuro-2a cells after a 24-h treatment with apoE, as determined by propidium iodide reactivity and flow cytometry. Each bar shows the

mean and standard deviation (n=8). Pre-incubated apoE4 was significantly more toxic than the tetramer at 0.15 and 0.03 mg/ml (Tukey test; p<0.05). **(c).** The effect of apoE tetramer on viability using the MTT assay. Data points show mean and standard deviation (n=24). ApoE4 tetramer was significantly more toxic than the control at 0.15 or 0.03 mg/ml (1-way ANOVA Dunnett test; p<0.05). ApoE3 was significantly toxic compared to the control only at 0.15 mg/ml (p<0.05). ApoE2 was not significantly toxic compared to the control at all concentrations (p>0.05). ApoE4 tetramer was significantly more toxic than apoE3 or apoE2 tetramer at 0.15 or 0.03 mg/ml (1-way ANOVA Tukey test; p<0.05). **(d).** The effect of pre-incubated apoE on viability using the MTT assay. Data points show mean and standard deviation (n=24). All isoforms were significantly toxic to the cells compared to the control at 0.03 or 0.15 mg/ml (Dunnett test; p<0.05). ApoE4 was significantly more toxic than apoE3 or apoE2 at 0.03 or 0.15 mg/ml (Tukey test; p<0.05). All pre-incubated isoforms were significantly more toxic than their tetrameric counterparts at 0.15 or 0.03 mg/ml (Tukey test; p<0.05).

Figure 7. ApoE mutants show a correlation between changes in conformational stability and aggregation rates. (a). Purified E255A-apoE4 tetramer (0.2 mg/ml), which lacks domain interaction, was incubated at 37 ^{o}C in AB buffer, and aliquots were analyzed by gel filtration chromatography at the indicated timepoints. **(b).** Purified R61T-apoE4 tetramer (0.2 mg/ml), which lacks domain interaction, was incubated at 37 ^{o}C in AB buffer, and aliquots were analyzed by gel filtration chromatography at the indicated time points. **(c).** Guanidine hydrochloride denaturation curves of apoE3, apoE4 and R61T-apoE4. Error bars indicate the standard deviation of three independent experiments. **(d).** Thioflavin T reactivity of low mass mouse apoE upon incubation at 37 ^{o}C. Each point represents the mean and standard deviation of three independently incubated samples. Data show wild-type mouse apoE and two "humanized" variants. Wild-type mouse apoE does not display domain interaction. T61R-mouse apoE displays domain interaction and has a similar conformational stability to wild-type mouse apoE. T61R, G83T, N113G mouse apoE displays domain interaction and a largely decreased conformational stability relative to wild-type mouse apoE.

Figure 8. Models of potential pathways influencing apoE aggregate formation. For both **(a)** and **(b)**, models (left) show an apoE molecule (within the tetramer context) as an amino-terminal four helix bundle and a carboxyl-terminal helix separated by a flexible linker. Partially destabilized apoE (middle) has been shown elsewhere to have a higher affinity for lipids. Our data suggest that this conformation also promotes aggregation. In **(a)**, the aggregate structure is modelled as an α-helix-rich amyloid protofibril with a minor fraction of protein forming the β-strands that stabilize the fibril core. In **(b)**, the aggregate structure is modelled as helix–helix interactions stabilizing the fibril.

Figure 1.

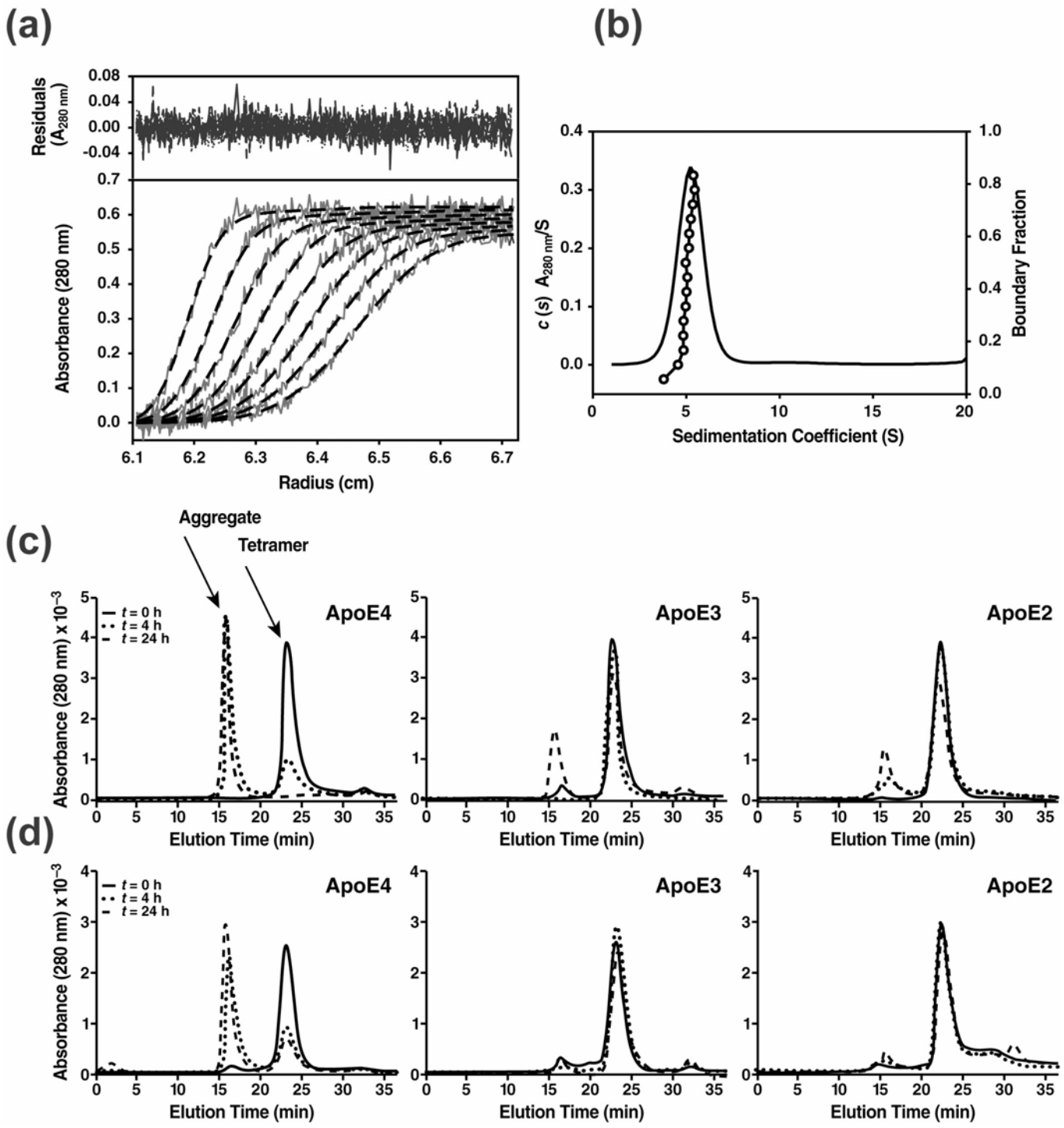
(a)
Residuals ($A_{280\ nm}$)
0.08
0.04
0.00
-0.04
Absorbance (280 nm)
0.7
0.6
0.5
0.4
0.3
0.2
0.1
0.0
6.1
6.2
6.3
6.4
6.5
6.6
6.7
Radius (cm)
(b)
c (s) $A_{280\ nm}$/S
0.4
0.3
0.2
0.1
0.0
1.0
0.8
0.6
0.4
0.2
0.0
Boundary Fraction
0
5
10
15
20
Sedimentation Coefficient (S)
(c)
Aggregate
Tetramer
Absorbance (280 nm) x 10^{-3}
t = 0 h
t = 4 h
t = 24 h
ApoE4
ApoE3
ApoE2
Elution Time (min)
(d)
Absorbance (280 nm) x 10^{-3}
t = 0 h
t = 4 h
t = 24 h
ApoE4
ApoE3
ApoE2
Elution Time (min)

Figure 2.

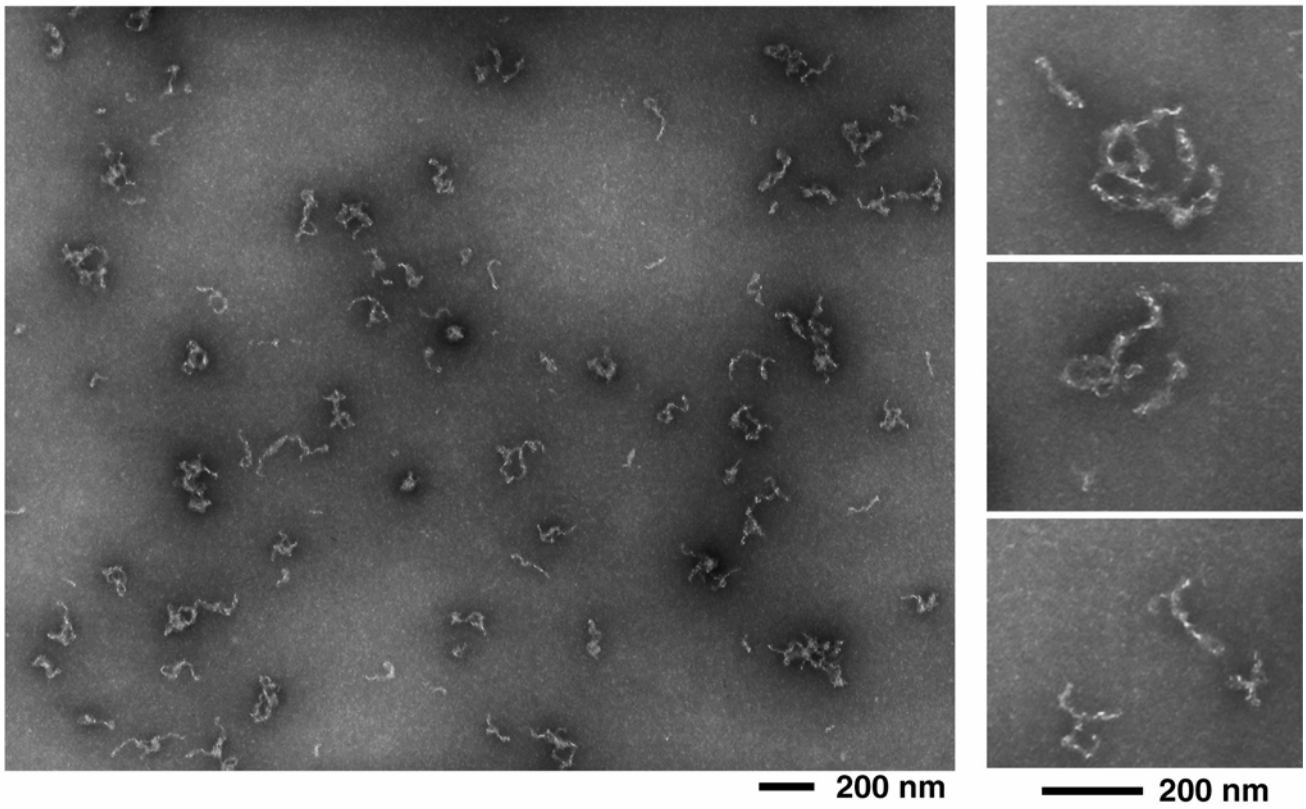

Figure 3.

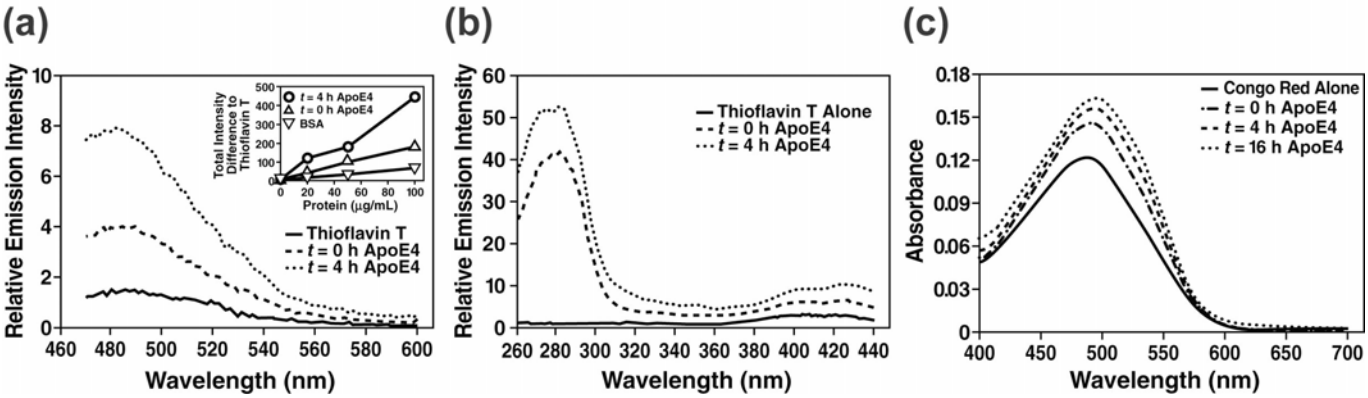
(a)
(b)
(c)
Relative Emission Intensity
Wavelength (nm)
Thioflavin T
t = 0 h ApoE4
t = 4 h ApoE4
Total Intensity Difference to Thioflavin T
BSA
Protein (μg/mL)
Thioflavin T Alone
Absorbance
Congo Red Alone
t = 16 h ApoE4

Figure 4.

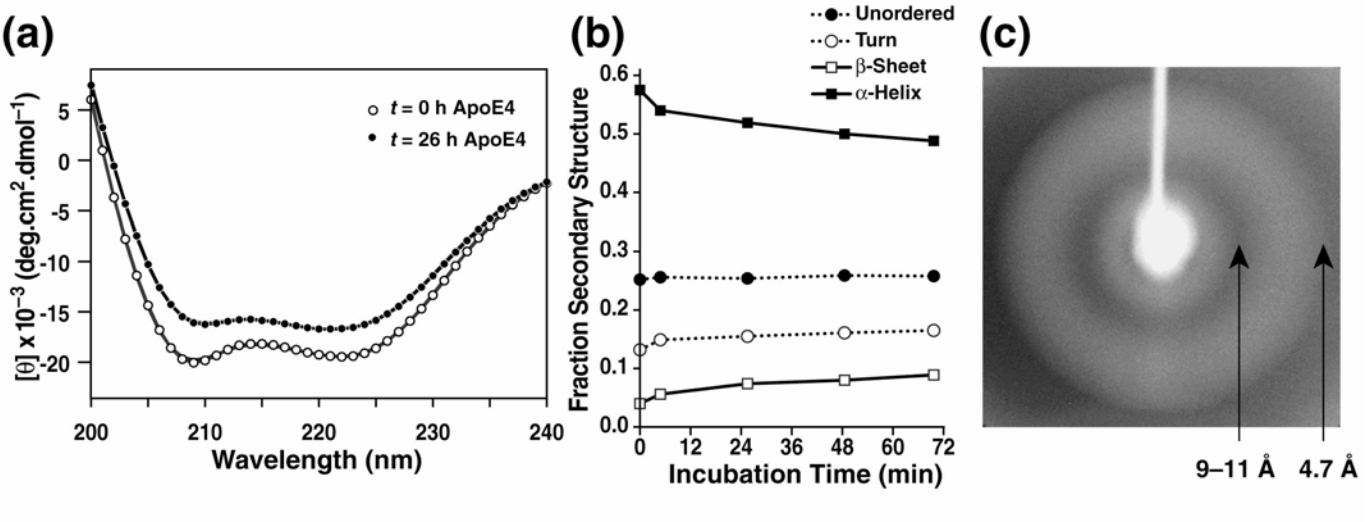
(a)
t = 0 h ApoE4
t = 26 h ApoE4
[θ] x 10^-3 (deg.cm^2.dmol^-1)
5
0
-5
-10
-15
-20
200
210
220
230
240
Wavelength (nm)
(b)
Unordered
Turn
β-Sheet
α-Helix
Fraction Secondary Structure
0.6
0.5
0.4
0.3
0.2
0.1
0.0
0
12
24
36
48
60
72
Incubation Time (min)
(c)
9–11 Å
4.7 Å

Figure 5.

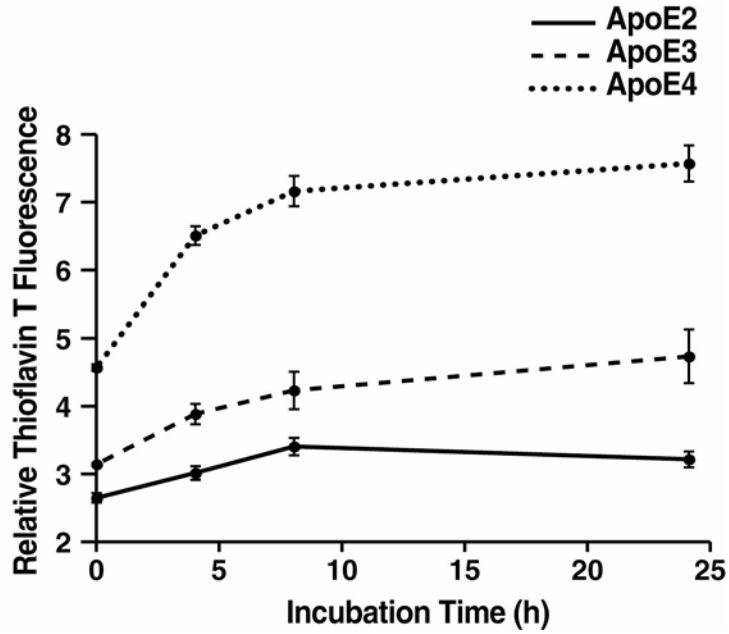
ApoE2
ApoE3
ApoE4
Relative Thioflavin T Fluorescence
8
7
6
5
4
3
2
0
5
10
15
20
25
Incubation Time (h)

Figure 6.

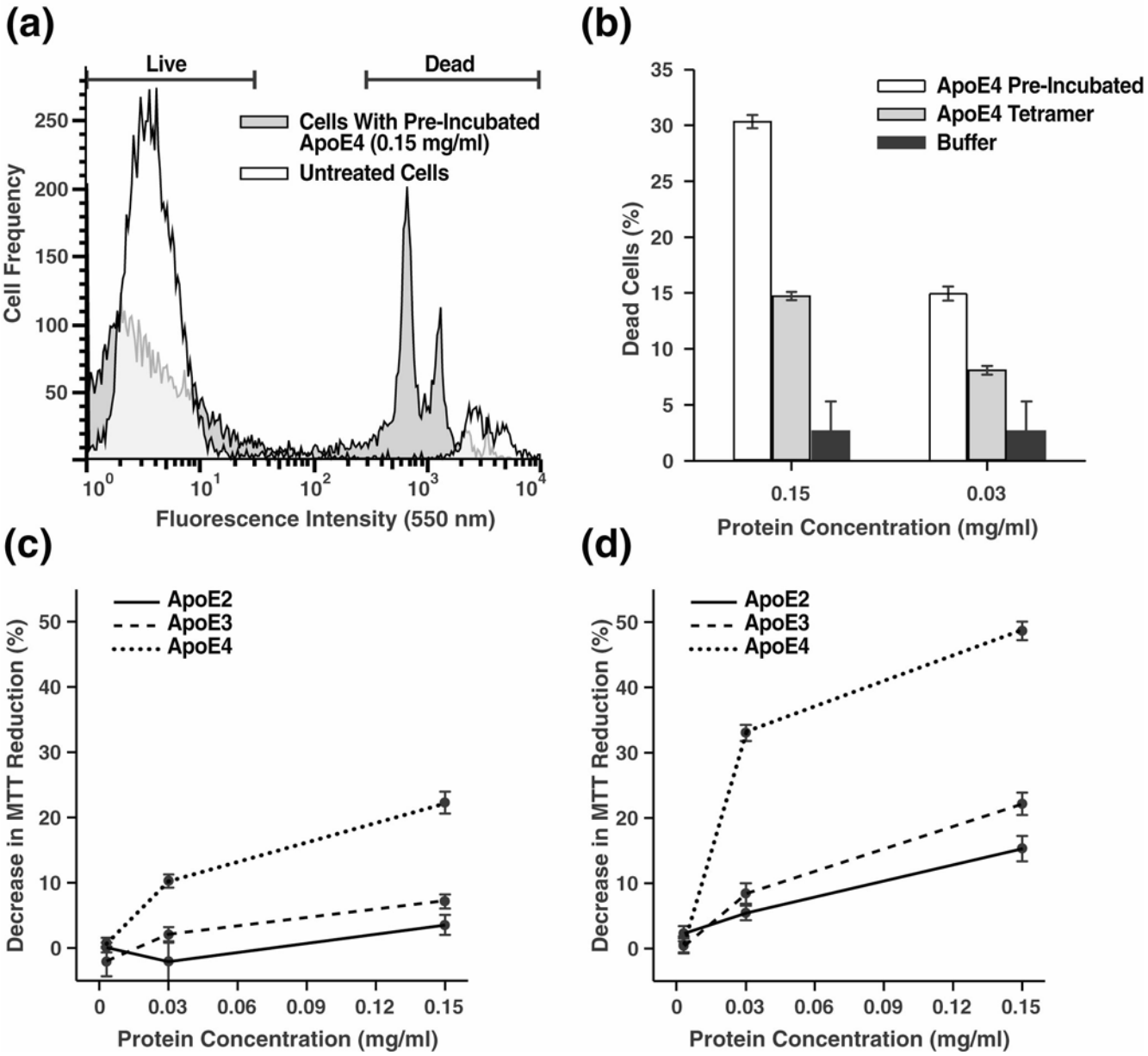
(a)
Live
Dead
Cells With Pre-Incubated ApoE4 (0.15 mg/ml)
Untreated Cells
Cell Frequency
Fluorescence Intensity (550 nm)
(b)
ApoE4 Pre-Incubated
ApoE4 Tetramer
Buffer
Dead Cells (%)
Protein Concentration (mg/ml)
(c)
ApoE2
ApoE3
ApoE4
Decrease in MTT Reduction (%)
Protein Concentration (mg/ml)
(d)
ApoE2
ApoE3
ApoE4
Decrease in MTT Reduction (%)
Protein Concentration (mg/ml)

Figure 7.

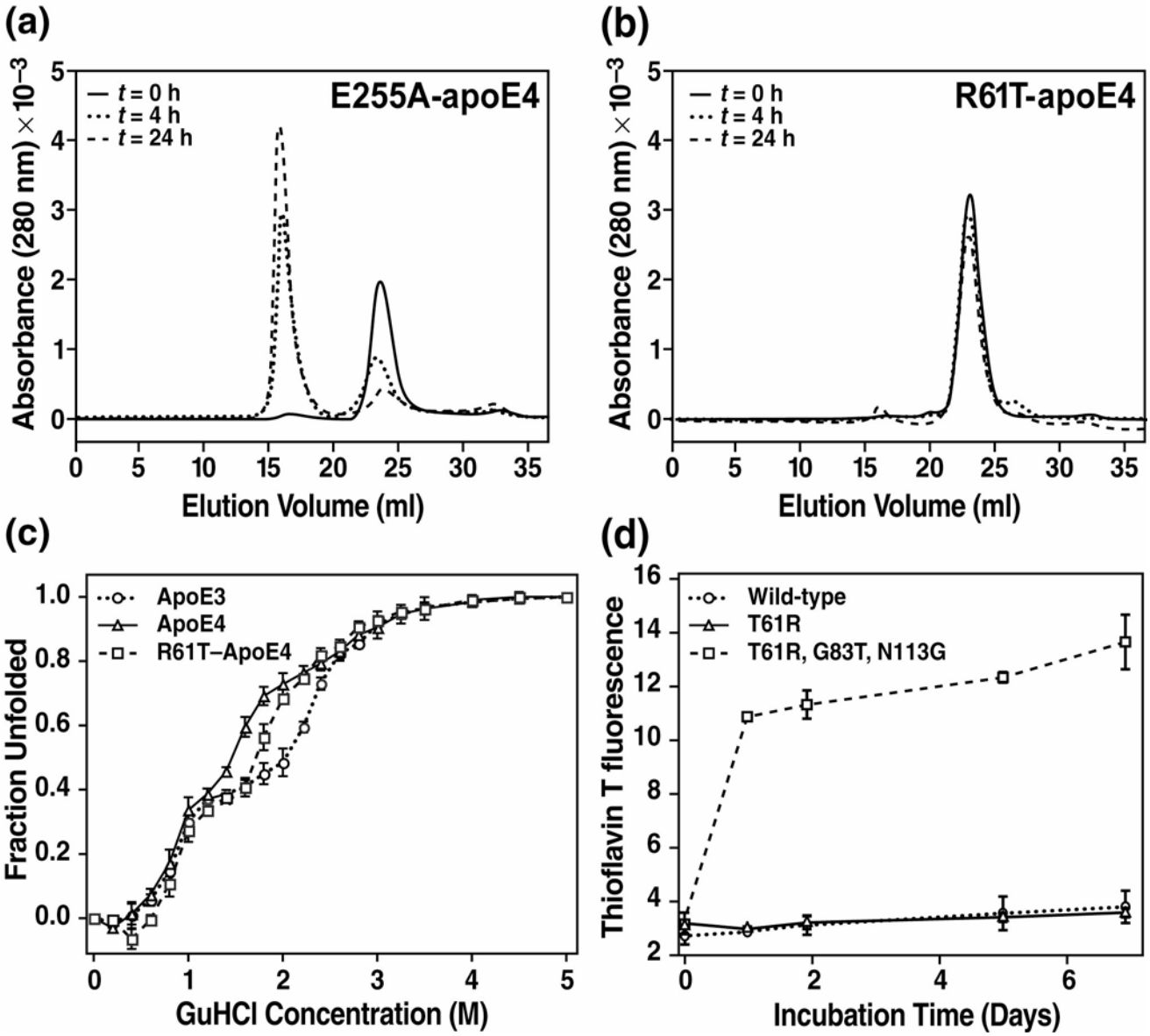
(a)
E255A-apoE4
t = 0 h
t = 4 h
t = 24 h
Absorbance (280 nm) × 10−3
Elution Volume (ml)
(b)
R61T-apoE4
t = 0 h
t = 4 h
t = 24 h
Absorbance (280 nm) × 10−3
Elution Volume (ml)
(c)
ApoE3
ApoE4
R61T–ApoE4
Fraction Unfolded
GuHCl Concentration (M)
(d)
Wild-type
T61R
T61R, G83T, N113G
Thioflavin T fluorescence
Incubation Time (Days)

Figure 8.

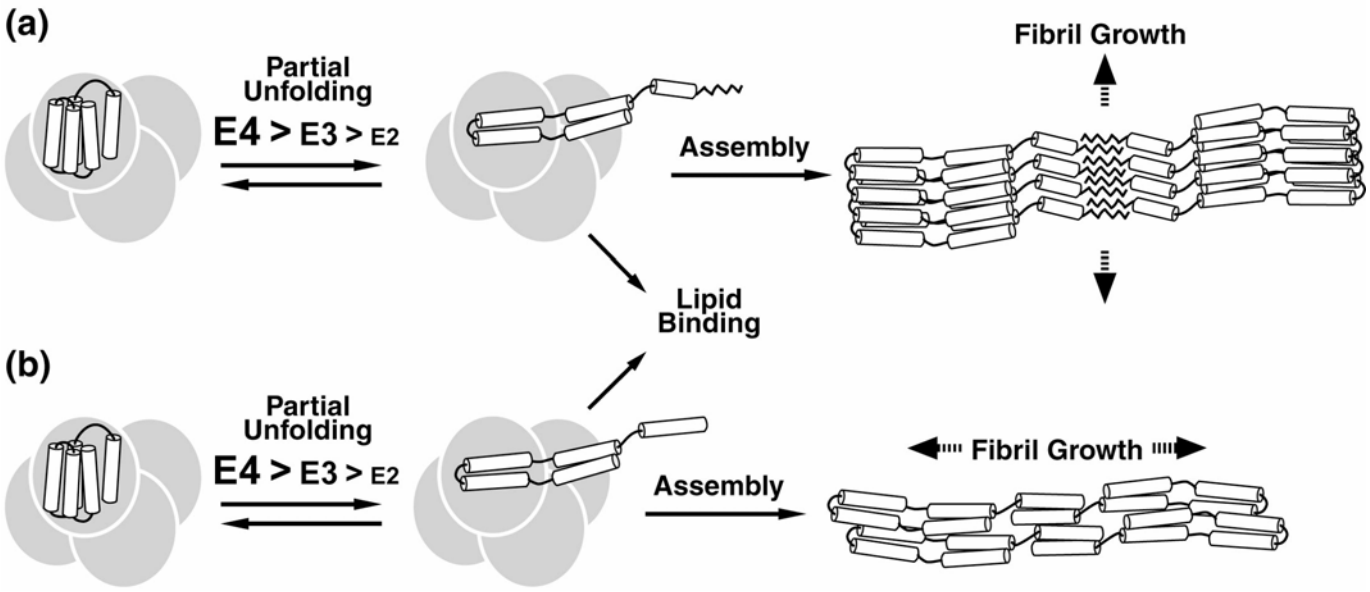
(a)
Partial
Unfolding
E4 > E3 > E2
Assembly
Fibril Growth
Lipid
Binding
(b)
Partial
Unfolding
E4 > E3 > E2
Assembly
Fibril Growth